Original Article

Insights into the relationship between mitral annular dimensions, derived sphincter-like features and systolic longitudinal excursion of the mitral annular plane in healthy adults from the MAGYAR-Healthy Study

Attila Nemes, Nóra Ambrus, Csaba Lengyel

Department of Medicine, Albert Szent-Györgyi Medical School, University of Szeged, Szeged, Hungary

Contributions: (I) Conception and design: A Nemes; (II) Administrative support: N Ambrus; (III) Provision of study materials or patients: A Nemes; (IV) Collection and assembly of data: A Nemes; (V) Data analysis and interpretation: A Nemes; (VI) Manuscript writing: All authors; (VII) Final approval of manuscript: All authors.

Correspondence to: Attila Nemes, MD, PhD, DSc. Department of Medicine, Albert Szent-Györgyi Medical School, University of Szeged, Semmelweis street 8, P.O. Box 427, H-6725 Szeged, Hungary. Email: nemes.attila@med.u-szeged.hu.

Background: The mitral annulus (MA) is a fibrous ring with a three-dimensional (3D) movement during the cardiac cycle having an up-and-town longitudinal motion and a sphincter-like narrowing-dilating pattern respecting the cardiac cycle. In the clinical practice, the MA plane systolic excursion (MAPSE), a feature of MA longitudinal function, can be assessed by the simple and widely used M-mode echocardiography (MME), while changes of MA dimensions and derived functional properties can be accurately measured by 3D speckle-tracking echocardiography (3DSTE) at the same time. The aim of the present retrospective cohort study was to evaluate the associations between MME-derived MAPSE and 3DSTE-derived MA dimensions in healthy adults for better understanding their physiologic relationship.

Methods: The subject group of 137 consecutive healthy individuals (34.8±12.3 years, 66 males) was classified into subgroups regarding their mean ± standard deviation (SD) of MAPSE and end-diastolic and end-systolic MA diameters (MAA-D and MAA-S, respectively). Cut-offs for MAPSE (11 and 17 mm), MAA-D (5.31 and 9.59 cm^2) and MAA-S (2.36 and 4.62 cm^2) were used to create the subgroups of subjects with less than mean – SD, mean and larger than mean + SD.

Results: None of the MA dimensions (MAA-D: 7.07±2.20 *vs.* 7.40±2.03 *vs.* 8.00±2.34 cm^2, P=non-significant (ns) for all; MAA-S: 3.43±1.04 *vs.* 3.42±1.11 *vs.* 3.77±1.21 cm^2, P=ns for all) and derived functional properties differed significantly between the subgroups based on MAPSE. With increasing MAA-D, MAPSE did not change (13.8±2.9 *vs.* 14.0±2.9 *vs.* 14.6±3.1 mm, P=ns for all), while other MA dimensions and MA fractional area change showed a parallel increase. With increasing MAA-S, MA dimensions increased, while derived MA functional properties showed a parallel decrease with preserved MAPSE (14.4±2.5 *vs.* 13.9±2.8 *vs.* 14.5±3.7 mm, P=ns for all).

Conclusions: MME-derived MAPSE and 3DSTE-derived MA dimensions and derived functional 'sphincter-like' properties are not associated in healthy adults.

Keywords: Echocardiography; healthy; speckle-tracking; three-dimensional (3D); mitral annulus (MA)

Submitted Dec 03, 2024. Accepted for publication Mar 21, 2025. Published online Apr 28, 2025.
doi: 10.21037/qims-2024-2731
View this article at: https://dx.doi.org/10.21037/qims-2024-2731

Introduction

The mitral valve is a hyperbolic paraboloid and saddle-shaped, three-dimensional (3D) complex structure integrating its annulus [mitral annulus (MA)], anterior and posterior leaflets and papillary muscles with tendineal chords (1-5). The MA is a fibrofatty ring having a 3D movement during the cardiac cycle with an up-and-town longitudinal motion and a sphincter-like narrowing-dilating pattern respecting the cardiac cycle similarly to the tricuspid annulus (TA) (1-11). In the clinical practice, the MA plane systolic excursion (MAPSE), a feature of MA longitudinal function, can be assessed by the simple and widely used M-mode echocardiography (MME) (7-9,12), while changes of MA dimensions and derived functional properties can be accurately measured by 3D speckle-tracking echocardiography (3DSTE) at the same time (10). The exact relationship between these functional properties has never been assessed, not even in healthy circumstances. Therefore, our aim was to measure and compare the relationship of MME-derived MAPSE and 3DSTE-derived MA dimensions in healthy adults for better understanding their physiologic relationship. We present this article in accordance with the STROBE reporting checklist (available at https://qims.amegroups.com/article/view/10.21037/qims-2024-2731/rc).

Methods

Study population

The present retrospective cohort study consisted of 137 consecutive healthy adult volunteers with a mean age of 34.8±12.3 years (66 males), who were involved in the study between 2011 and 2017. A subject was considered to be healthy if all routine echocardiographic parameters proved to be normal and were within the normal reference ranges. None of the subjects had any acute or chronic disorder, pathological state or other condition which could affect the findings. Drug was not used by any participant. No one was athlete, obese, smoker or performed yoga 1 week before the examination. Electrocardiographic (ECG) and laboratory findings did not confirm any pathology. Complete echocardiographic analysis included M-mode, two-dimensional (2D) and Doppler echocardiography with a negative result in all cases. All subjects with MME-derived MAPSE and 3DSTE-derived MA parameters were included into this analysis. 3DSTE-derived data acquisition was performed at the end of echocardiographic examination with a complete offline analysis at a later date. This substudy is a part of the Motion Analysis of the heart and Great vessels bY three-dimensionAl speckle-tRacking echocardiography in Healthy subjects (MAGYAR-Healthy) Study, which aimed, among others to find physiologic associations between clinical factors and 3DSTE-derived parameters ('Magyar' means 'Hungarian' in Hungarian language) (10,11,13). The study was conducted in accordance with the Declaration of Helsinki and its subsequent amendments. The Institutional and Regional Human Biomedical Research Committee of the University of Szeged approved the study (No. 71/2011), the approval was renewed every second year (latest approval: 17th March, 2025). Informed consent was given by all individuals.

2D Doppler echocardiography

2D Doppler echocardiography was performed in agreement with the professional guidelines and accepted practices (12). In all cases, routine echocardiographic studies were performed using a Toshiba Artida™ cardiac ultrasound tool attached to a PST-30BT (1–5 MHz) phased-array transducer. The examination was carried out in such a way that the subject was first asked to lie in her/his left lateral decubitus position. Then the transducer was placed on typical parasternal and apical positions on her/his chest. In parasternal long-axis view, left atrial and left ventricular (LV) dimensions, and thickness of the interventricular septum (IVS) and LV posterior wall (PW) were measured. The transducer was repositioned into typical apical position to measure LV volumes in apical 2-chamber (AP2CH) and 4-chamber (AP4CH) long-axis views and LV ejection fraction (EF) was calculated using the Simpson's method (12,14,15). Significant valvular regurgitation and stenosis were excluded by Doppler echocardiography and early (E) and late (A) diastolic mitral inflow velocities were measured by pulsed Doppler for LV diastolic function. To characterize LV longitudinal shortening and up-and-down motion of the MA as a movement of the lateral MA edge toward the LV apex in systole, MAPSE was also calculated. MAPSE measurements were adjusted for apical foreshortening and annular geometry (*Figure 1*) (12,15).

3D speckle-tracking echocardiography

Establishment of 3DSTE followed the accepted guidelines and practices (10,11,13,16-20). Following transducer change to a 3D echocardiography-capable PST-25SX matrix-array transducer, according to our practices and routines,

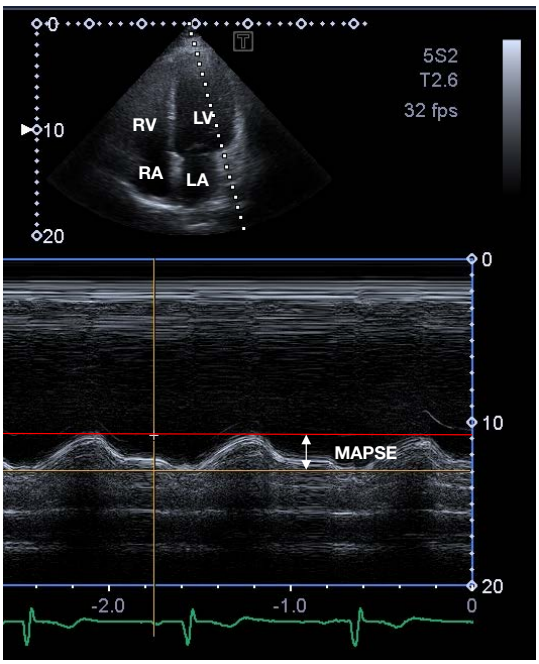

Figure 1 M-mode echocardiography-derived measurement of MAPSE in apical four-chamber long-axis view. LA, left atrium; LV, left ventricle; MAPSE, mitral annular plane systolic excursion; RA, right atrium; RV, right ventricle.

pyramid-shaped, 'full volume' 3D echocardiographic datasets were acquired from the apical window in all cases following image optimisations, which included definition of gain, magnitude, etc. Six constant RR intervals were required to acquire the images and the subject has to be in breath-hold during the acquisition. As a second step, acquired 3D datasets were analysed offline by the vendor-provided 3D Wall Motion Tracking software (Ultra Extend, Toshiba Medical Systems, Tokyo, Japan, version 2.7) at a later date. During this analysis, the software automatically selected AP2CH and AP4CH long-axis views and 3 short-axis views at apical, midventricular and basal LV levels at end-diastole. These long-axis views helped to find the optimal MA lateral and septal edges. On C7 short-axis view, cross-sectional 2D-projected view of MA has been presented. End-diastole was defined as a frame just before the mitral valve closure, while end-systole was defined as a frame just before the mitral valve opening. Using these end-diastolic and end-systolic MA morphological parameters, functional 'sphincter-like' features were calculated (*Figure 2*) (10,21):

MA morphological parameters

- MA diameter (MAD), evaluated by drawing a perpendicular line from the peak of MA curvature to the middle of the straight MA border;
- MA area (MAA), assessed by planimetry;
- MA perimeter (MAP), evaluated by planimetry.

MA functional properties

- MA fractional shortening (MAFS), defined as [(end-diastolic MAD – end-systolic MAD)/end-diastolic MAD] × 100%;
- MA fractional area change (MAFAC), defined as [(end-diastolic MAA – end-systolic MAA)/end-diastolic MAA] × 100%.

Statistical analysis

Mean ± standard deviation (SD) and n (%) formats were used for continuous and categorical data, respectively. A P value less than 0.05 was considered to be statistically significant. Student's *t*-test and Mann-Whitney Wilcoxon test were used for datasets in accordance with their distribution. One-way analysis of variance (ANOVA) test with Bonferroni correction was used, where appropriate. For categorical variables, Fisher's exact test was performed. Pearson's coefficients were measured featuring correlations between variables. The Bland-Altman method was used to determine intraobserver and interobserver agreements. For intraobserver and interobserver correlations, intraclass correlation coefficients (ICCs) were calculated. SPSS software (version No. 22, SPSS Inc., Chicago, IL, USA) was used during statistical analyses.

Results

Demographic data

Routine clinical parameters were within the normal reference ranges including weight (72.1±12.1 kg), height (170.4±10.1 cm), body surface area (1.83±0.24 m^2), body mass index (BMI) (23.7±2.2 kg/m^2), systolic blood pressure (121.8±4.5 mmHg), and diastolic blood pressure (74.6±4.4 mmHg).

Classification of subjects

The subject group of 137 healthy individuals was classified into subgroups in accordance with the value of mean ± SD of MAPSE and end-diastolic MAA (MAA-D) and end-systolic MAA (MAA-S). Cut-offs for MAPSE (11 and 17 mm), MAA-D (5.31 and 9.59 cm^2) and MAA-S (2.36 and 4.62 cm^2)

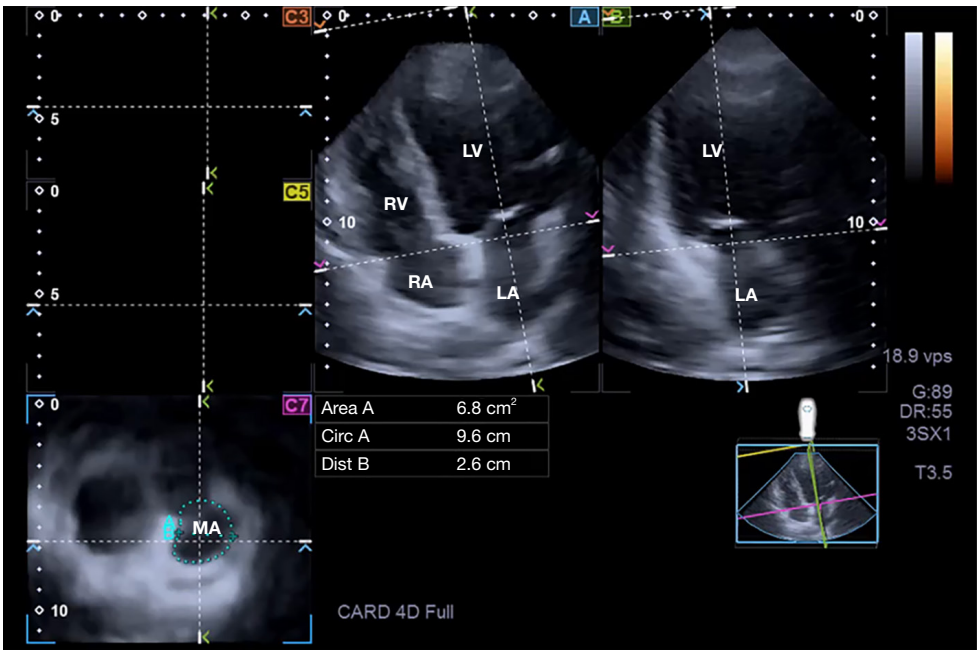

Figure 2 Three-dimensional speckle-tracking echocardiographic measurement of the mitral annulus: apical four-chamber (A) and two-chamber (B) long-axis views and cross-sectional view (C7) of the mitral annulus optimised on (A) and (B) long-axis views. Area, mitral annular area; Circ, mitral annular perimeter; Dist, mitral annular diameter; LA, left atrium; LV, left ventricle; MA, mitral annulus; RA, right atrium; RV, right ventricle.

were used to create subgroups of subjects with less than mean – SD, mean and larger than mean + SD.

2D Doppler echocardiography

All routine 2D echocardiographic parameters including LA diameter (37.4±3.7 mm), end-diastolic LV diameter (48.1±3.6 mm) and volume (107.1±27.8 mL), end-systolic LV diameter (32.2±3.5 mm) and volume (38.1±10.4 mL), thickness of the IVS (9.2±1.2 mm) and LV-PW (9.4±1.5 mm) and LV ejection fraction (64.7%±3.6%) were all within the normal reference ranges. None of the 2D echocardiographic data differed significantly between the subgroups examined, except for IVS (8.70±1.17 *vs.* 9.73±1.24 mm, P=0.01) and LV-PW (8.77±1.22 *vs.* 10.06±1.24 mm), which proved to be less thickened in subject with MAA-D ≤5.31 cm^2 *vs.* MAA-D ≥9.59 cm^2. Larger than grade 1 valvular insufficiency or significant valvular stenosis on any valves could be excluded in all cases.

3D speckle-tracking echocardiography

None of the MA dimensions and derived functional properties differed significantly between the subgroups based on MAPSE. With increasing MAA-D, MAPSE did not change, other MA dimensions and MAFAC showed a parallel increase. With increasing end-systolic MAA (MAA-S), MA dimensions increased, while derived MA functional properties showed a parallel decrease with preserved MAPSE (*Tables 1-3*).

Correlations

Significant correlations between MAPSE and end-diastolic MAD (r=0.09, P=0.29), MAA (r=0.13, P=0.24), MAP (r=0.15, P=0.15), end-systolic MAD (r=0.003, P=0.98), MAA (r=0.13, P=0.22), MAP (r=0.13, P=0.22), MAFAC (r=0.06, P=0.59) and MAFS (r=0.07, P=0.49) could not be detected. No correlations were found between MAPSE and end-diastolic MAD not only for all, but being less than mean, mean and larger than mean as well (*Figure 3*).

Feasibility of 3DSTE- and MME-derived MA assessments

The study comprised 179 healthy individuals, from which 42 subjects were excluded due to insufficient image quality.

Table 1 Three-dimensional speckle-tracking echocardiography-derived mitral annular morphological and functional parameters in subgroups based on the value of mitral annular plane systolic excursion in healthy subjects

Data	All healthy subjects (n=137)	MAPSE ≤11 mm (n=24)[a]	11 mm< MAPSE <17 mm (n=88)[b]	MAPSE ≥17 mm (n=25)[c]
Mitral annular dimensions				
MAD-D (cm)	2.45±0.42	2.37±0.38	2.45±0.4	2.56±0.38
MAA-D (cm^2)	7.45±2.14	7.07±2.20	7.40±2.03	8.00±2.34
MAP-D (cm)	10.33±1.44	10.06±1.42	10.28±1.39	10.75±1.56
MAD-S (cm)	1.61±0.37	1.65±0.32	1.58±0.37	1.68±0.39
MAA-S (cm^2)	3.49±1.13	3.43±1.04	3.42±1.11	3.77±1.21
MAP-S (cm)	7.13±1.09	7.09±0.90	7.09±1.11	7.32±1.10
Mitral annular 'sphincter-like' functional properties				
MAFAC (%)	51.4±14.9	48.3±15.1	52.1±14.8	51.1±15.0
MAFS (%)	33.3±15.2	29.2±15.7	34.2±15.0	33.8±14.6
Mitral annular plane systolic excursion				
MAPSE (mm)	14.1±3.00	9.70±1.60	14.0±1.5*	18.3±1.2*#

The data are presented as mean ± standard deviation. *, P<0.0001: *vs*. group a; #P<0.0001: *vs*. group b. MAFAC, mitral annular fractional area change; MAFS, mitral annular fractional shortening; MAA-D, end-diastolic mitral annular area; MAA-S, end-systolic mitral annular area; MAD-D, end-diastolic mitral annular diameter; MAD-S, end-systolic mitral annular diameter; MAP-D, end-diastolic mitral annular perimeter; MAP-S, end-systolic mitral annular perimeter; MAPSE, mitral annular plane systolic excursion.

Table 2 Three-dimensional speckle-tracking echocardiography-derived mitral annular morphological and functional parameters in subgroups based on the value of end-diastolic mitral annular area in healthy subjects

Data	All healthy subjects (n=137)	MAA-D, cm^2			P value		
		≤5.31 (n=24)[a]	>5.31 to <9.59 (n=90)[b]	≥9.59 (n=23)[c]	b *vs*. a	c *vs*. a	c *vs*. b
Mitral annular dimensions							
MAD-D (cm)	2.45±0.42	1.99±0.22	2.45±0.34	2.93±0.32	<0.0001	<0.0001	<0.0001
MAA-D (cm^2)	7.45±2.14	4.54±0.65	7.29±1.08	10.94±1.06	<0.0001	<0.0001	<0.0001
MAP-D (cm)	10.33±1.44	8.19±0.52	10.32±0.76	12.47±0.72	<0.0001	<0.0001	<0.0001
MAD-S (cm)	1.61±0.37	1.44±0.22	1.60±0.38	1.81±0.36	0.049	0.0002	0.019
MAA-S (cm^2)	3.49±1.13	2.70±0.65	3.47±1.13	4.38±0.81	0.002	<0.0001	0.0005
MAP-S (cm)	7.13±1.09	6.30±0.85	7.13±1.05	8.04±0.68	0.0006	<0.0001	0.0002
Mitral annular 'sphincter-like' functional properties							
MAFAC (%)	51.4±14.9	40.4±13.4	51.9±15.0	59.7±8.4	0.001	<0.0001	0.019
MAFS (%)	33.3±15.2	27.0±11.5	34.0±15.5	37.1±15.2	0.043	0.015	0.390
Mitral annular plane systolic excursion							
MAPSE (mm)	14.1±3.00	13.8±2.9	14.0±2.9	14.6±3.1	0.689	0.357	0.422

The data are presented as mean ± standard deviation. MAFAC, mitral annular fractional area change; MAFS, mitral annular fractional shortening; MAA-D, end-diastolic mitral annular area; MAA-S, end-systolic mitral annular area; MAD-D, end-diastolic mitral annular diameter; MAD-S, end-systolic mitral annular diameter; MAP-D, end-diastolic mitral annular perimeter; MAP-S, end-systolic mitral annular perimeter; MAPSE, mitral annular plane systolic excursion.

Table 3 Three-dimensional speckle-tracking echocardiography-derived mitral annular morphological and functional parameters in subgroups based on the value of end-systolic mitral annular area in healthy subjects

Data	All healthy subjects (n=137)	MAA-S, cm^2			P value		
		≤2.36 (n=23)[a]	>2.36 to <4.62 (n=91)[b]	≥4.62 (n=23)[c]	b *vs*. a	c *vs*. a	c *vs*. b
Mitral annular dimensions							
MAD-D (cm)	2.45±0.42	2.17±0.32	2.46±0.43	2.72±0.31	0.003	<0.0001	0.008
MAA-D (cm^2)	7.45±2.14	6.10±1.73	7.40±2.09	9.02±1.63	0.007	<0.0001	0.0009
MAP-D (cm)	10.33±1.44	9.47±1.31	10.28±1.4	11.35±1.07	0.013	<0.0001	0.001
MAD-S (cm)	1.61±0.37	1.20±0.13	1.59±0.27	2.12±0.24	<0.0001	<0.0001	<0.0001
MAA-S (cm^2)	3.49±1.13	1.98±0.22	3.40±0.62	5.34±0.51	<0.0001	<0.0001	<0.0001
MAP-S (cm)	7.13±1.09	5.55±0.39	7.13±0.65	8.71±0.50	<0.0001	<0.0001	<0.0001
Mitral annular 'sphincter-like' functional properties							
MAFAC (%)	51.4±14.9	64.9±9.9	51.1±13.8	38.9±11.9	<0.0001	<0.0001	0.0002
MAFS (%)	33.3±15.2	43.6±9.8	33.8±14.7	20.9±12.4	0.003	<0.0001	0.0002
Mitral annular plane systolic excursion							
MAPSE (mm)	14.1±3.0	14.4±2.5	13.9±2.8	14.5±3.7	0.463	0.896	0.399

The data are presented as mean ± standard deviation. MAFAC, mitral annular fractional area change; MAFS, mitral annular fractional shortening; MAA-D, end-diastolic mitral annular area; MAA-S, end-systolic mitral annular area; MAD-D, end-diastolic mitral annular diameter; MAD-S, end-systolic mitral annular diameter; MAP-D, end-diastolic mitral annular perimeter; MAP-S, end-systolic mitral annular perimeter; MAPSE, mitral annular plane systolic excursion

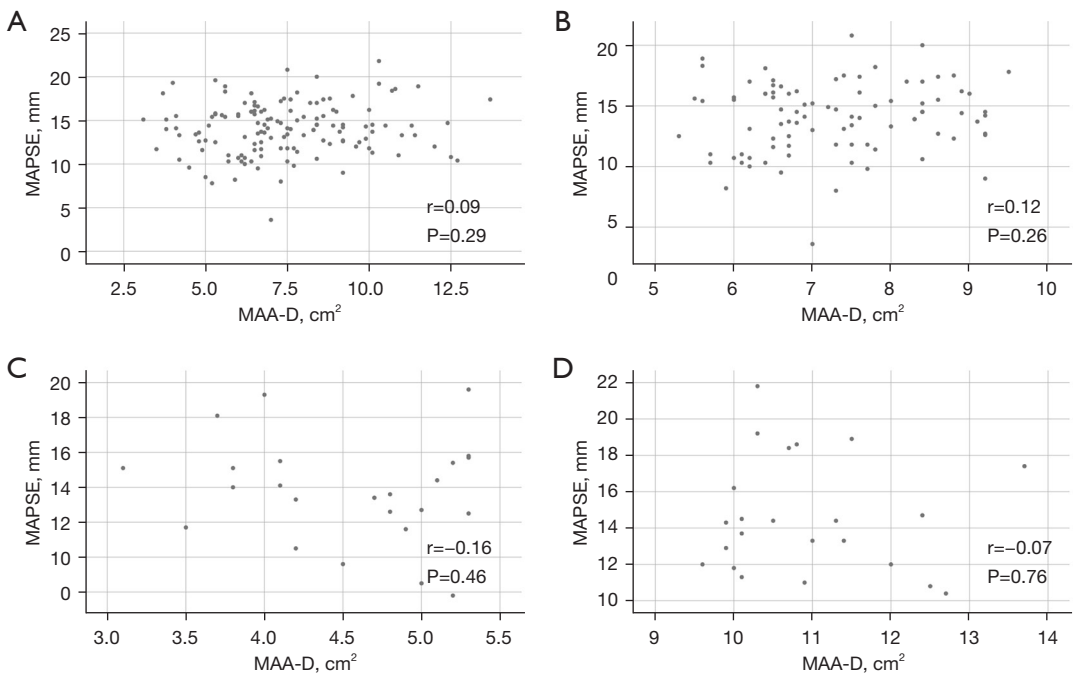

Figure 3 Correlations between mitral annular plane systolic excursion and end-diastolic mitral annular area for all (A), being mean (B), less than mean (C) or larger than mean (D). MAA-D, end-diastolic mitral annular area; MAPSE, mitral annular plane systolic excursion.

Table 4 Intra- and interobserver variability for three-dimensional speckle-tracking echocardiography-derived mitral annular dimensions and mitral annular plane systolic excursion

Parameters	Intraobserver agreement			Interobserver agreement		
	Mean ± 2SD	ICC	P value	Mean ± 2SD	ICC	P value
End-diastolic MAD (cm)	0.03±0.15	0.94	<0.0001	0.03±0.26	0.97	<0.0001
End-diastolic MAA (cm^2)	−0.04±0.67	0.97	<0.0001	0.04±0.45	0.96	<0.0001
End-diastolic MAP (cm)	−0.03±0.74	0.97	<0.0001	−0.08±0.65	0.97	<0.0001
End-systolic MAD (cm)	−0.03±0.13	0.96	<0.0001	0.03±0.12	0.98	<0.0001
End-systolic MAA (cm^2)	−0.04±0.21	0.96	<0.0001	−0.04±0.89	0.96	<0.0001
End-systolic MAP (cm)	0.08±0.65	0.97	<0.0001	0.06±0.56	0.97	<0.0001
MAPSE (cm)	0.01±0.04	0.99	<0.0001	0.02±0.04	0.99	<0.0001

Intraobserver agreement: by 2 measurements of the same observer. Interobserver agreement: by 2 measurements of two independent observers. ICC, interclass correlation coefficient; MAA, mitral annular area; MAD, mitral annular diameter; MAP, mitral annular perimeter; MAPSE, mitral annular plane systolic excursion; SD, standard deviation.

Therefore, the overall feasibility was 76.5%. There were no differences in involved (n=137) and excluded (n=42) subjects in age (34.8±12.3 *vs.* 33.9±11.3 years, P=ns), male gender (n=66, 48% *vs.* n=21, 50%, P=ns) and BMI (23.7±2.2 *vs.* 24.2±2.4 kg/m^2, P=ns). None of the subjects had any arrhythmia.

Reproducibility of 3DSTE-derived MA assessments

3DSTE-derived end-systolic and end-diastolic MA diameter, area, and perimeter measured 2 times by the same examiner (intraobserver agreement) and by two independent examiners (interobserver agreement) were shown as mean ± 2SD together with respective ICCs in *Table 4*. Measurements were performed in 35 randomly selected healthy individuals. All reproducibility measurements were performed blindly.

Discussion

In recent decades there has been a huge development in cardiovascular imaging. In addition to MME and 2D echocardiography, which have already been used and widespread, new echocardiographic techniques appeared, such as the novel 3DSTE enabling to accurately assess end-diastolic and end-systolic MA dimensions (12,16-20). Moreover, MAFS and MAFAC are considered to be derived properties of MA sphincter-like function (10,21). MME-derived MAPSE assessment is an accepted and validated method for LV functional evaluation and considered to be a significant prognosticator as well (7-9). Its clinical significance has been examined in several circumstances and disorders (22,23). However, the relationship between MME-derived MAPSE and 3DSTE-derived MA dimensions and 'sphincter-like' functional properties has not been assessed in healthy individuals.

MA is a fibrous, saddle-shaped structure with a dynamic motion respecting the cardiac cycle, which 3D movement is highly dependent on adjacent LV (and left atrial) function as suggested by previous works (1,2,6). There is a systolic circumferential (sphincter-like) MA contraction due to the shortening of the LV basal helical fibers, which plays an important role in leaflet coaptation (1). These sort of changes in MA dimensions can be quantified by 3D echocardiography-derived measurements (10,21). However, in systole, the MA folds across its intercommissural axis ("saddle-deepening") as well, which promotes coaptation without producing leaflet distortion ("wrinkling") (1,24-26). LV contraction causes an apical displacement of the entire MA, the degree of displacement of the anterior and posterior parts is unequal. The anterior MA translates less than the posterior due to its tethering to the aortic root. Therefore, the anterior part of the MA moves posteriorly, bringing the MA anterior and posterior poles closer together (1,27). In the present study, MAPSE was used as a simple MME-based functional feature representing MA longitudinal motion towards the LV apex during the cardiac cycle. In recent 3DSTE studies, significant associations could be demonstrated between LV deformation and rotational mechanics and MA 'sphincter-like' function

(28,29). Moreover, MA and TA dimensions and 'sphincter-like' features were also compared (30). Only LV longitudinal contraction represented by LV longitudinal strain (LS) and MAPSE was found to be associated, LV strains in other directions were not related to MAPSE in healthy adults (13). According to these facts, we could ask how MAPSE, MA dimensions and sphincter-like features are related to each other in healthy circumstances.

In the present study, no associations could be detected between MAPSE, a representative of MA longitudinal displacement, MA dimensions and derived MAFS and MAFAC. It is even more interesting in light of the fact that it is looked at it in comparison with the right heart. In a recent study, tricuspid annular plane systolic excursion (TAPSE) and similar TA sphincter-like features like TA fractional shortening (TAFS) and TA fractional area change (TAFAC) were compared in healthy circumstances (11). Increased TAPSE was associated with increased TAFAC due to reduced end-systolic TA area. Similar associations could not be detected for MA. It would be interesting to know the reason for this difference. Theoretically it could be explained by several facts. There are differences in LV and right ventricular (RV) myocardial architecture: while LV has left-handed subepicardial and right-handed subendocardial myocardial fibers running perpendicularly to each other, superficial circumferential RV fibers run parallel to the TA are responsible for the bellows effect of the RV and deep RV muscle fibers are responsible for the longitudinal TA movement, characterised by MME-derived TAPSE. The structure of the left and right atria, the number of leaflets of the MA and that of the TA and related morphology are also different. Moreover, the role of MA-related 'saddle-deepening' should not be excluded either. However, further physiologic studies are warranted to confirm the findings and to see these relationships in early stages of valvular incompetencies.

Limitation section

- First of all it should be considered that measurements were performed in the 2D plane-projected image of MA, but its special 3D saddle-shape was not considered.
- MME typically operates at a high frame rate (65±5 fps), offering superior temporal resolution for capturing rapid annular motion like MAPSE, whereas 3DSTE has a lower frame rate (31±1 fps), which may limit its ability not only to track peak annular excursion accurately, but all measurements are affected by this technical issue. In order to be able to perform measurements even more accurately during 3DSTE, a higher frame rate is an essential requirement. Moreover, 3DSTE-derived lower image quality is also related to larger transducers, stitching/motion artifacts during data analysis, etc. as well (16-20).
- Although 3DSTE is useful for more complex analysis of heart chambers and valves, the present study did not purpose such measurements over the evaluation of the MA. Moreover, comparison of 2D echocardiography versus 3DSTE in the evaluation of MA was also not aimed to be performed.
- It would have been interesting to compare 3DSTE-derived MA measurements against those measured with other imaging techniques. This sort of analysis could even be a subject of future investigations.
- Although there is a technical opportunity for speckle-tracking-based assessment of MA function, this sort of analysis was not aimed in this study.
- The overall feasibility of the study proved to be only 76.5%, which could significantly affect findings.
- It was examined whether the excluded subjects differed systematically from the final cohort (e.g., older age, higher BMI, arrhythmias) and how this might introduce selection bias into the results. However, basic characteristics of the involved and excluded subjects did not differ.
- It could not be stated with 100% certainty that all subjects were healthy. More tests would have increased the certainty of the lack of any abnormalities.

Conclusions

MME-derived MAPSE and 3DSTE-derived MA dimensions and derived functional 'sphincter-like' properties are not associated in healthy adults.

Acknowledgments

None.

Footnote

Reporting Checklist: The authors have completed the STROBE reporting checklist. Available at https://qims.amegroups.com/article/view/10.21037/qims-2024-2731/rc

Funding: None.

Conflicts of Interest: All authors have completed the ICMJE uniform disclosure form (available at https://qims.amegroups.com/article/view/10.21037/qims-2024-2731/coif). A.N. serves as an unpaid editorial board member of *Quantitative Imaging in Medicine and Surgery*. The other authors have no conflicts of interest to declare.

Ethical Statement: The authors are accountable for all aspects of the work in ensuring that questions related to the accuracy or integrity of any part of the work are appropriately investigated and resolved. The study was conducted in accordance with the Declaration of Helsinki and its subsequent amendments. The Institutional and Regional Human Biomedical Research of the University of Szeged approved the study (No. 71/2011). Informed consent was given by all patients.

References

1. Silbiger JJ. Anatomy, mechanics, and pathophysiology of the mitral annulus. Am Heart J 2012;164:163-76.
2. Silbiger JJ, Bazaz R. The anatomic substrate of mitral annular contraction. Int J Cardiol 2020;306:158-61.
3. Ho SY. Anatomy of the mitral valve. Heart 2002;88 Suppl 4:iv5-10.
4. Levine RA, Handschumacher MD, Sanfilippo AJ, Hagege AA, Harrigan P, Marshall JE, Weyman AE. Three-dimensional echocardiographic reconstruction of the mitral valve, with implications for the diagnosis of mitral valve prolapse. Circulation 1989;80:589-98.
5. Salgo IS, Gorman JH 3rd, Gorman RC, Jackson BM, Bowen FW, Plappert T, St John Sutton MG, Edmunds LH Jr. Effect of annular shape on leaflet curvature in reducing mitral leaflet stress. Circulation 2002;106:711-7.
6. Mihaila S, Muraru D, Miglioranza MH, Piasentini E, Peluso D, Cucchini U, Iliceto S, Vinereanu D, Badano LP. Normal mitral annulus dynamics and its relationships with left ventricular and left atrial function. Int J Cardiovasc Imaging 2015;31:279-90.
7. Hu K, Liu D, Herrmann S, Niemann M, Gaudron PD, Voelker W, Ertl G, Bijnens B, Weidemann F. Clinical implication of mitral annular plane systolic excursion for patients with cardiovascular disease. Eur Heart J Cardiovasc Imaging 2013;14:205-12.
8. Hensel KO, Roskopf M, Wilke L, Heusch A. Intraobserver and interobserver reproducibility of M-mode and B-mode acquired mitral annular plane systolic excursion (MAPSE) and its dependency on echocardiographic image quality in children. PLoS One 2018;13:e0196614.
9. Cirin L, Crișan S, Luca CT, Buzaș R, Lighezan DF, Văcărescu C, Cozgarea A, Tudoran C, Cozma D. Mitral Annular Plane Systolic Excursion (MAPSE): A Review of a Simple and Forgotten Parameter for Assessing Left Ventricle Function. J Clin Med 2024;13:5265.
10. Nemes A, Kormányos Á, Domsik P, Kalapos A, Gyenes N, Lengyel C. Normal reference values of three-dimensional speckle-tracking echocardiography-derived mitral annular dimensions and functional properties in healthy adults: Insights from the MAGYAR-Healthy Study. J Clin Ultrasound 2021;49:234-9.
11. Nemes A, Rácz G, Kormányos Á, Ruzsa Z, Achim A, Lengyel C. The Relationship between Tricuspid Annular Longitudinal and Sphincter-like Features of Its Function in Healthy Adults: Insights from the MAGYAR-Healthy Study. Life (Basel) 2023;13:2079.
12. Lang RM, Badano LP, Mor-Avi V, Afilalo J, Armstrong A, Ernande L, Flachskampf FA, Foster E, Goldstein SA, Kuznetsova T, Lancellotti P, Muraru D, Picard MH, Rietzschel ER, Rudski L, Spencer KT, Tsang W, Voigt JU. Recommendations for cardiac chamber quantification by echocardiography in adults: an update from the American Society of Echocardiography and the European Association of Cardiovascular Imaging. J Am Soc Echocardiogr 2015;28:1-39.e14.
13. Nemes A, Ambrus N, Lengyel C. Three-Dimensional Speckle-Tracking Echocardiography-Derived Left Ventricular Global Longitudinal Strain and Mitral Annular Plane Systolic Excursion Are Associated in Healthy Adults-Insights from the MAGYAR-Healthy Study. Biomedicines 2025;13:625.
14. Nemes A, Forster T. Recent echocardiographic examination of the left ventricle – from M-mode to 3D speckle-tracking imaging. Orv Hetil 2015;156:1723-40.
15. Feigenbaum H. editor. Echocardiography. 5th edition. Philadelphia, PA, USA: Lea & Febiger; 1994.
16. Franke A, Kuhl HP. Second-generation real-time 3D

echocardiography: a revolutionary new technology. Medica Mundi 2003;47:34-40.
17. Ammar KA, Paterick TE, Khandheria BK, Jan MF, Kramer C, Umland MM, Tercius AJ, Baratta L, Tajik AJ. Myocardial mechanics: understanding and applying three-dimensional speckle tracking echocardiography in clinical practice. Echocardiography 2012;29:861-72.
18. Urbano-Moral JA, Patel AR, Maron MS, Arias-Godinez JA, Pandian NG. Three-dimensional speckle-tracking echocardiography: methodological aspects and clinical potential. Echocardiography 2012;29:997-1010.
19. Muraru D, Niero A, Rodriguez-Zanella H, Cherata D, Badano L. Three-dimensional speckle-tracking echocardiography: benefits and limitations of integrating myocardial mechanics with three-dimensional imaging. Cardiovasc Diagn Ther 2018;8:101-17.
20. Gao L, Lin Y, Ji M, Wu W, Li H, Qian M, Zhang L, Xie M, Li Y. Clinical Utility of Three-Dimensional Speckle-Tracking Echocardiography in Heart Failure. J Clin Med 2022;11:6307.
21. Anwar AM, Soliman OII, ten Cate FJ, Nemes A, McGhie JS, Krenning BJ, van Geuns RJ, Galema TW, Geleijnse ML. True mitral annulus diameter is underestimated by two-dimensional echocardiography as evidenced by real-time three-dimensional echocardiography and magnetic resonance imaging. Int J Cardiovasc Imaging 2007;23:541-7.
22. Jarori U, Maatman TK, Maatman B, Mastouri R, Sawada SG, Khemka A. Mitral Annular Plane Systolic Excursion: An Early Marker of Mortality in Severe COVID-19. J Am Soc Echocardiogr 2020;33:1411-3.
23. Matos JD, Balachandran I, Heidinger BH, Mohebali D, Feldman SA, McCormick I, Litmanovich D, Manning WJ, Carroll BJ. Mitral annular plane systolic excursion and tricuspid annular plane systolic excursion for risk stratification of acute pulmonary embolism. Echocardiography 2020;37:1008-13.
24. Lawrie GM. Structure, function, and dynamics of the mitral annulus: importance in mitral valve repair for myxamatous mitral valve disease. Methodist Debakey Cardiovasc J 2010;6:8-14.
25. Kaplan SR, Bashein G, Sheehan FH, Legget ME, Munt B, Li XN, Sivarajan M, Bolson EL, Zeppa M, Arch MZ, Martin RW. Three-dimensional echocardiographic assessment of annular shape changes in the normal and regurgitant mitral valve. Am Heart J 2000;139:378-87.
26. Tibayan FA, Rodriguez F, Langer F, Zasio MK, Bailey L, Liang D, Daughters GT, Ingels NB Jr, Miller DC. Annular remodeling in chronic ischemic mitral regurgitation: ring selection implications. Ann Thorac Surg 2003;76:1549-54; discussion 1554-5.
27. Komoda T, Hetzer R, Oellinger J, Sinlawski H, Hofmeister J, Hübler M, Felix R, Uyama C, Maeta H. Mitral annular flexibility. J Card Surg 1997;12:102-9.
28. Kovács Z, Kormányos Á, Domsik P, Kalapos A, Lengyel C, Ambrus N, Ajtay Z, Piros GÁ, Forster T, Nemes A. Left ventricular longitudinal strain is associated with mitral annular fractional area change in healthy subjects-Results from the three-dimensional speckle tracking echocardiographic MAGYAR-Healthy Study. Quant Imaging Med Surg 2019;9:304-11.
29. Nemes A, Kovács Z, Kormányos Á, Domsik P, Kalapos A, Ajtay Z, Lengyel C. Left ventricular apical rotation is associated with mitral annular function in healthy subjects. Results from the three-dimensional speckle-tracking echocardiographic MAGYAR-Healthy Study. Physiol Int 2020;107:145-54.
30. Nemes A, Kormányos Á, Lengyel C. Comparison of dimensions and functional features of mitral and tricuspid annuli in the same healthy adults: insights from the three-dimensional speckle-tracking echocardiographic MAGYAR-Healthy Study. Quant Imaging Med Surg 2024;14:6780-91.

Cite this article as: Nemes A, Ambrus N, Lengyel C. Insights into the relationship between mitral annular dimensions, derived sphincter-like features and systolic longitudinal excursion of the mitral annular plane in healthy adults from the MAGYAR-Healthy Study. Quant Imaging Med Surg 2025;15(5):4748-4757. doi: 10.21037/qims-2024-2731

